Solar Energy Materials and Solar Cells 194 (2019) 130–136

Contents lists available at ScienceDirect

Solar Energy Materials and Solar Cells

journal homepage: www.elsevier.com/locate/solmat

Degradation and fault diagnosis of photovoltaic cells using impedance spectroscopy

Noboru Katayama*, Suguru Osawa, Shunya Matsumoto, Takuma Nakano, Mutsumi Sugiyama

Department of Electrical Engineering, Tokyo University of Science, Noda, Chiba 278-8510, Japan

ARTICLE INFO

Keywords:
Photovoltaic cell
Diagnosis tool
Impedance spectroscopy

ABSTRACT

Impedance spectroscopy is widely employed to evaluate electrochemical devices, and our group has been proposing its use as a novel diagnosis tool for photovoltaic modules. In this study, photovoltaic cells are subjected to several types of failure and degradation that frequently occur in polycrystalline photovoltaic cells, such as mechanical stress, interconnect ribbon disconnection, and potential-induced degradation. The impedance characteristics of these cells are measured as Nyquist plots, in addition to the current-voltage (I-V) characteristics to compare the characteristics among the failure modes and demonstrate the applicability of impedance spectroscopy as a potential photovoltaic module diagnosis tool. The equivalent circuit parameters, with and without failure and degradation, are obtained from the impedance characteristics and compared. The influence of bias voltage and temperature on the impedance characteristics are investigated prior to failure and degradation. The application of mechanical stress decreases the parallel resistance and moves the right edge of the Nyquist plot further inside the exact semicircle, while interconnection ribbon disconnection also decreases the parallel resistance and increases the series resistance, and potential-induced degradation decreases both the parallel resistance and capacitance.

1. Introduction

Photovoltaic cells are becoming popular as renewable energy sources and the number of installed photovoltaic power systems is increasing significantly worldwide. There are many countries that have introduced a feed-in tariff policy to accelerate investment in photovoltaic cell power generation. As a result, various types and scales of photovoltaic power plants have been built to date. Although solar cells are generally considered to be maintenance-free, there have been reported cases of failure.

Microcracks are small breakages on photovoltaic cells mainly caused by mechanical stress. Mechanical stress originates from installation strain, exogenous shock and thermal stress from the temperature cycling of day and night, or variations of solar radiation. In most cases, moderate microcracks have very little impact on the performance of the photovoltaic cells that the degradation would not be found easily; however, if microcracks are allowed to become larger, then they may cause converged current paths in a specific area or a short circuit. Another result of microcracks is snail trails, or snail tracks [1–7]. These appear as discolorations near microcracks on the surface of the cells. Moisture from the air permeates through the backsheet and the microcracks to ionize the silver finger electrodes. Diffused silver ions then react chemically and cause snail trails. Snail trails also appear at the edges of photovoltaic cells. An investigation on the influence of snail trails on the power generation has revealed that, depending on the defect level, the maximum power of photovoltaic modules can be reduced by 10–30% [7].

The disconnection of interconnection ribbons is one of the well-known failures in photovoltaic modules [8]. Multiple interconnect ribbons are used to connect photovoltaic cells in series and are soldered onto the screen printed contacts of the photovoltaic cells. Failures of the interconnection in most cases are caused by degradation of the soldering due to temperature cycling [9]. Ribbon disconnection does not lead to critical failure of an entire system if other ribbons between the cells connected by the failed ribbon, usually one or two, remain intact to conduct electric current. However, if all the ribbons between the same cells are disconnected, then the photovoltaic array cannot deliver the electric power and the module has failed. However, performance degradation due to the disconnection of interconnection ribbons is usually small, so that it is difficult to detect a failure without electroluminescence methods.

Potential-induced degradation (PID) is caused by large voltage differences between the photovoltaic cells and the system ground connected with the module frame. Photovoltaic modules are typically

* Corresponding author.
E-mail address: katayama@rs.tus.ac.jp (N. Katayama).

https://doi.org/10.1016/j.solmat.2019.01.040
Received 23 September 2018; Received in revised form 21 January 2019; Accepted 29 January 2019
Available online 16 February 2019
0927-0248/ © 2019 Elsevier B.V. All rights reserved.

connected in series, which is referred to as a string, to generate high voltage. The voltage between the cells and the module frame allows sodium ions in the front glass to move into the cell through encapsulation materials. Sodium ions that reach the cell induce leakage current and degrade the performance [10–13,15–19].

Despite such various problems, some photovoltaic power plant owners do not even notice a decline in their system power output, because it is dependent on the amount of solar radiation and temperature, which varies with time and season. Considering such background and the increase in the number of photovoltaic power plants, there is an increasing demand for the diagnosis of photovoltaic systems and modules.

Measurement of the current-voltage (I-V) characteristics is one of the simplest diagnosis methods and is widely utilized for practical applications and in fundamental research. I-V curves directly provide information on the performance of photovoltaic cells, strings and arrays. The maximum power outputs measured with instruments such as I-V curve tracers are compared with those estimated by calculation from solar radiation and temperature measurements. Analytical methods for I-V curves have also been proposed. For example, a partial malfunction in a module appears as distortions of the I-V curves [20,21].

The detection of hotspots with thermal imaging cameras is a convenient method to scan photovoltaic arrays and is an effective tool for large-scale arrays. A cell that is incapable of power generation acts as a resistor and produces Joule heat, which results in hotspots when other cells generate electricity, and this can be easily observed even remotely [22,23].

Electroluminescence methods are used in the manufacturing process. Under forward bias conditions, photovoltaic cells emit infrared radiation, which is then detected with a CCD camera. The defect areas of a cell are displayed dark, so that hidden cracks and small dead spots can be detected [24,25].

The time domain reflectometry method has been recently introduced, which uses the response when an electrical pulse is applied from the end of the photovoltaic array to detect which photovoltaic module in the string is defective. A portable detector for such measurements has already been developed and commercialized. Time domain reflectometry can also be used for the detection of ground-faults [26].

All of these methods can be used to detect the presence of defects or the location of a problem, and lately used to provide information regarding failure modes, i.e., the type of failure that has occurred [27]. Degradation such as PID advances slowly and gradually degrades the power outputs, so that the photovoltaic modules do not necessarily have to be replaced urgently. On the other hand, degradation such as the disconnection of interconnection ribbons may cause sudden failure of power generation.

As a potential diagnosis tool for photovoltaic modules, we have been proposing the use of impedance spectroscopy. Impedance spectroscopy has long been a common analytical tool for the diagnosis of electrochemical devices, including lead-acid batteries, lithium-ion batteries, fuel cells, and dye-sensitized photovoltaic cells. Impedance spectroscopy has recently been applied for the fundamental analysis of semiconductor photovoltaic cells, such as evaluation of the depletion layer thickness and defects around the pn interface [28], sputtering damage around the pn interface [29] and estimation of the defect activation energy [30]. Several reports show applicability of impedance spectroscopy as a diagnosis tool for failures of photovoltaic modules and cells such as PID [31] and failure of finger electrodes [32]. The first example shows change in impedance characteristics for photovoltaic modules of which performance are decreased in an actual power plant. The second used acid vapor to make failure of finger electrodes on bare photovoltaic cells and found another time constant due to the failure. Impedance spectroscopy can provide the information not only for fault mode classification but also for the intensity of the faults. From the obtained impedance spectra, the parameters of the equivalent circuits

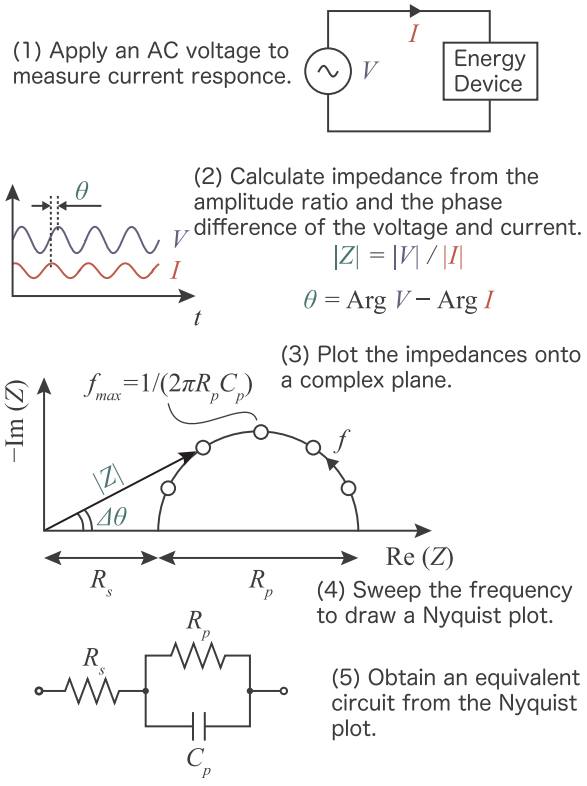

Fig. 1. Schematic diagram of impedance spectroscopy measurement.

are obtained, which are related to intensity of the intensity of the faults. However, there are no reports that shows impedance characteristics of various kinds of artificially-produced failures and analyze the parameters of the equivalent circuits in detail.

In this study, we first investigate the influence of DC bias voltage and temperature, which are important parameters for impedance spectroscopy, on the impedance characteristics. Next, common failure and degradation are applied to photovoltaic cells and the impedance characteristics are measured, in addition to the I-V characteristics, which are generally used for the diagnosis of photovoltaic power plants.

2. Impedance spectroscopy for photovoltaic cells

Impedance spectroscopy is widely used in electrochemical research on batteries and fuel cells to acquire information regarding these devices. Fig. 1 shows a schematic diagram that outlines impedance spectroscopy measurements. Although photovoltaic cells generate DC electricity as with other electrochemical energy devices, the addition of a small AC voltage at a certain frequency onto the DC voltage of the photovoltaic cell produces an AC current response at the same frequency. The impedance at that frequency is obtained from the AC voltage and current. Scanning the frequency range and plotting the impedance for each frequency on a complex plane gives a Nyquist plot. Parameter fitting of the Nyquist plot then produces the parameters for an equivalent circuit. The parameters change according to physical changes in a photovoltaic cell, or in a photovoltaic module that consists of photovoltaic cells, interconnect ribbons, by-pass diodes, and cable.

3. Experimental method

Commercially available polycrystalline silicon photovoltaic cells were used in this study (Fig. 2). The cells have a dimensions of 156 × 156 mm^2. Three bus bars and fingers are located on the surface of a cell. In a commercial photovoltaic module, the photovoltaic cells are interconnected by flat wire or metal ribbons and are connected in series.

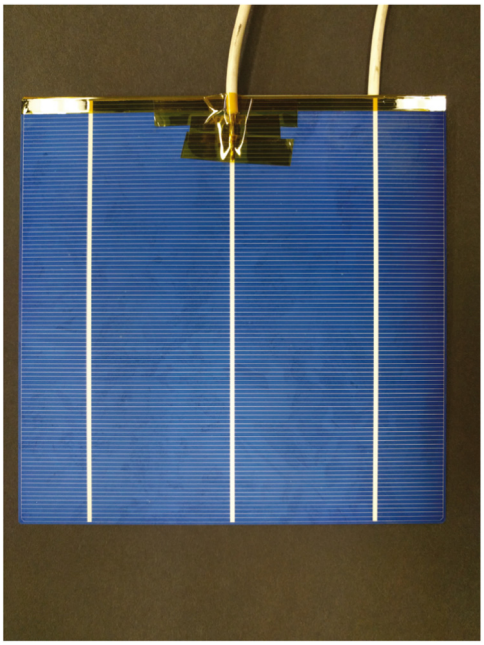

Fig. 2. Polycrystalline photovoltaic cell with wires soldered.

Bare photovoltaic cells were used and the wires were soldered onto the bus bar and backside, as shown in Fig. 2. The photovoltaic cells were subjected to mechanical stress tests, interconnection ribbon disconnection tests and PID tests, from which typical faults arise in photovoltaic modules.

Both impedance and I-V characteristics were measured for the photovoltaic cells from each test. An impedance analyzer (IM3590, Hioki E.E. Corporation), which can apply DC voltage for impedance measurements of batteries, was employed to measure the impedance. The amplitude of the AC voltage was 0.01 V, the frequency was swept from 0.1 Hz to 100 kHz, and the DC bias voltage was 0.1 V. Larger AC voltages improve the measurement resolution because signal-to-noise ratio is reduced but may deteriorate linearity. The AC voltage was optimized through preliminary tests so that appropriate accuracy could be obtained. In this study, a range of AC voltages was tried, and as a result, it turned out that the AC voltage of 0.01 V is the best for accuracy and precision. Photovoltaic cells were placed under dark conditions to avoid any characteristic changes due to photo-induced electron and irradiation noise.

The I-V characteristics were measured under dark conditions using a power supply (PBZ40-10, Kikusui Electronics Corp.) connected with a personal computer. The I-V characteristics influence the maximum power output directly and are frequently used for the diagnosis of photovoltaic devices. The applicability of impedance spectroscopy as a diagnosis tool for photovoltaic cells is demonstrated by comparison of the impedance characteristics with the I-V characteristics for various photovoltaic cell fault modes. The experimental conditions for each fault mode are detailed in the following subsection.

Although a constant DC bias voltage of 0.1 V is used to investigate the effect of cell failure upon the impedance characteristics, the DC bias voltage is an important parameter for impedance spectroscopy because it influences the pn junction condition and also changes the impedance characteristics. In addition, other types of failure may be detected by changing the DC bias voltage, which will be addressed in future work. The relationship between the DC bias voltage and the impedance characteristics was elucidated. The cell voltages were changed from 0.00 to 0.45 V, which are near the rated voltage of the cell used in this study.

The temperature of photovoltaic modules in photovoltaic power plants changes with the solar radiation and ambient temperature, and this influences impedance spectroscopy measurements. For practical use, the impedance characteristics should be compensated using the temperature. Therefore, measurement of the impedance characteristics under all possible cell temperatures is required. The impedance characteristics were thus measured for the temperature range from −20 °C to 50 °C.

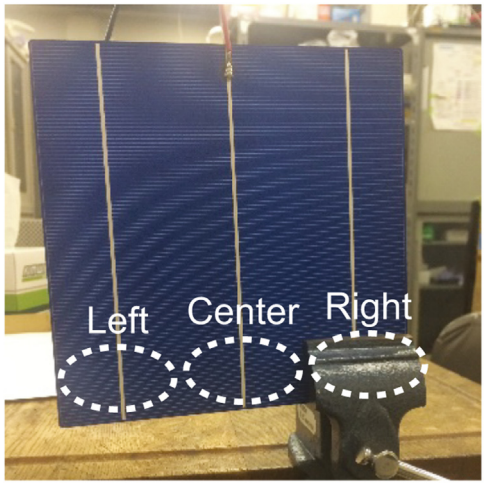

Fig. 3. Photograph of the mechanical stress test and the areas where mechanical stress is applied.

3.1. Mechanical stress test

One of the most reported failures in photovoltaic cells is microcracks, which are caused by mechanical stress. Microcracks in a cell have a small impact on the overall cell performance in most cases. However, the form of cracks may cause critical performance degradation. For example, potential induced degradation is advanced due to micro-cracks [14].

To reproduce mechanical stress, a vise was used to apply a stress of 6.34 kg/cm^2 at three different areas on the same photovoltaic cell. Fig. 3 shows the areas where the mechanical stress was applied. The area of the applied stress was 40 mm × 15 mm and rubber sheets were placed between the photovoltaic cell and the vice to apply uniform stress. The order of the position where the mechanical stress was applied was right, center and left, and impedance measurements were made after each stress application under dark conditions. The stress was measured with a stress sensor (FSR402, Interlink Electronics Inc.), of which the electrical resistance changes according to the applied stress.

3.2. Interconnect ribbon disconnection test

Two or three interconnect ribbons are typically used for each series connection between photovoltaic cells. If all the interconnect ribbons are disconnected, then the photovoltaic module cannot output electrical current.

In this study, we investigate whether changing the number of interconnect ribbons affects the impedance characteristics. Instead of actual interconnect ribbons, conducting wires were used for the test. The wires were soldered onto the respective bus bars, and disconnection of the interconnect ribbons were reproduced by changing which wires are connected to the measurement instruments.

3.3. Potential-induced degradation test

PID proceeds slowly and differentiation of its performance degradation from other types of degradation is difficult. Thus, the detection of PID is an important challenge.

The PID test was conducted using the following protocol. Fig. 4

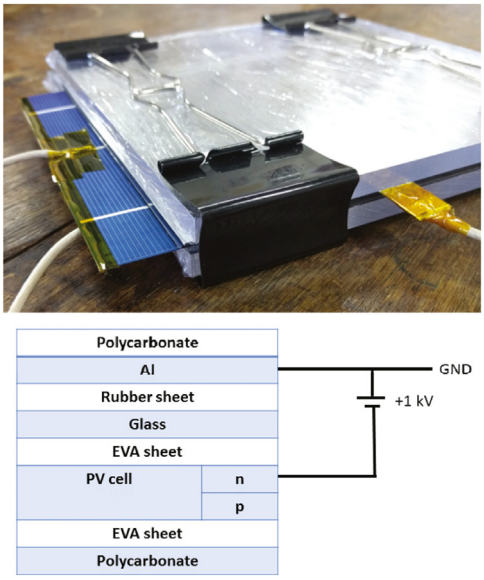

Fig. 4. Photograph (above) and cross-sectional diagram (below) of the PID test.

shows a photograph of the PID test setup and a schematic diagram of the test cell cross-section. A bare photovoltaic cell, two ethylene-vinyl acetate (EVA) sheets, a glass plate, a conductive rubber sheet and an aluminum plate are sandwiched between a pair of polycarbonate plates. EVA is a typical encapsulant film, which protects the photovoltaic cell from physical impact, water, dirt and UV-aging. Sodium ions from glass pass through the EVA and cause PID; white glass (B720) and soda-lime glass were used for the test. White glass has high transmittance in the visible wavelength range and is widely used for photovoltaic modules. Soda-lime glass is relatively inexpensive and commonly used as a window glass, although it contains a large amount of sodium ions. A negative voltage of − 1.0 kV is applied to the photovoltaic cell against the aluminum plate. The aluminum plate plays a role as the frame of the photovoltaic module, and it is grounded. The conductive rubber sheet ensures the contact between the aluminum plate and glass, which stabilizes the electric field. The temperature of the test cell was maintained at 85 °C using a constant-temperature oven.

The impedance characteristics and the I-V characteristics of the cells were obtained periodically. Even during these measurements, the cell temperature was maintained at 85 °C to avoid cell degradation by temperature cycling.

4. Results and discussion

Figs. 5 and 6 show the equivalent circuit parameters for the polycrystalline silicon photovoltaic cell as the DC bias voltage and the cell temperature are respectively changed. These parameters are calculated by curve-fitting of the obtained Nyquist plots. The equivalent circuit for the curve-fitting is shown in Fig. 1, which consists of a series resistance R_s, a parallel resistance R_p, and a parallel capacitance C_p, because the Nyquist plot shape is a single semicircle due to the uniform pn junction of polycrystalline photovoltaic cells. R_s is almost zero and is not shown in Figs. 5 and 6. R_p and C_p vary significantly with to the DC bias voltage. In practical use, the DC bias voltage can be controlled and fixed precisely at a specific voltage. R_p and C_p also vary with the temperature, although the range of variation is much smaller than that with change of the DC bias voltage. The cell temperature in the photovoltaic cells differs every time the diagnosis is performed. Therefore, the equivalent circuit parameters obtained in practical application must be compensated according to the measured temperature.

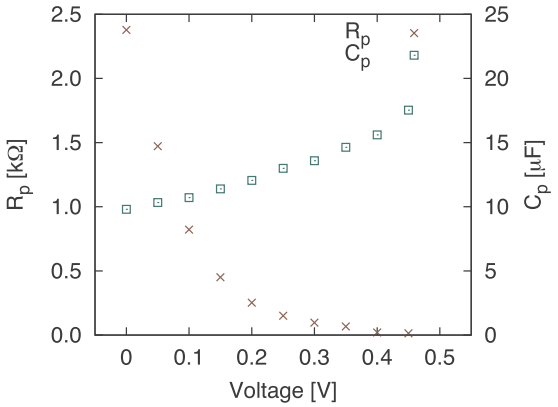

Fig. 5. Equivalent circuit parameters for the polycrystalline silicon photovoltaic cell as a function of DC bias voltage.

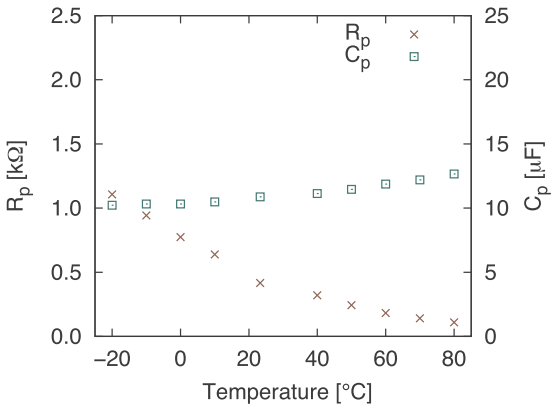

Fig. 6. Equivalent circuit parameters for the polycrystalline silicon photovoltaic cell as a function of cell temperature.

4.1. Mechanical stress test

Fig. 7 shows the I-V curves, Nyquist plots, and the equivalent circuit parameters for the photovoltaic cells with mechanical stress applied. The characteristics of the pristine photovoltaic cell before application of mechanical stress (Reference) are also shown. The equivalent circuit parameters are obtained by parameter fitting of the Nyquist plots. Although the cell emitted a small cracking sound when mechanical stress was applied to the cell each time, the cell showed no cracks on its surface. However, small cracks may exist in the cell that cannot be observed from the surface. Despite only slight changes in the I-V characteristics, the Nyquist plots showed significant shrinkage each time mechanical stress was applied. The equivalent circuit parameters indicate that the parallel resistance R_p, is decreased, as expected from the shrinkage of the Nyquist plot. On the other hand, the parallel capacitance C_p, remained constant. R_p is expressed with the differential resistance, which is calculated from the following equation:

$$R_p = \frac{dV}{dI} = \left(\frac{q}{kT} I_s e^{\frac{qV}{kT}}\right)^{-1} \quad (1)$$

where V and I are the forward voltage and current, q is the charge of an electron, k is the Boltzmann constant, T is the temperature, and I_s is the saturation current. However, R_p is also affected by the leakage current through the pn junction, and becomes smaller at higher defect levels of the pn junction or other causes of current conduction loss. In this case, crack formation increase the leakage current and R_p is decreased as a result.

It is noteworthy that the lower frequency range end (ca. <0.2 Hz) of the Nyquist plots deforms and moves further inside the original semicircle. The similar phenomenon has also been reported in the literature

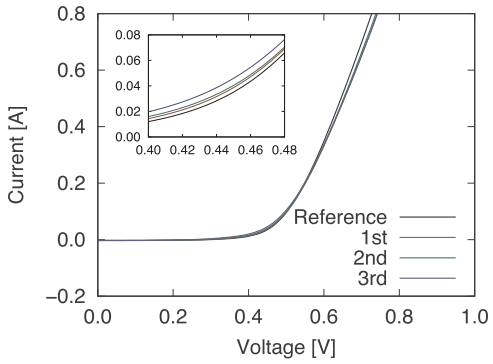

(a) I-V characteristics

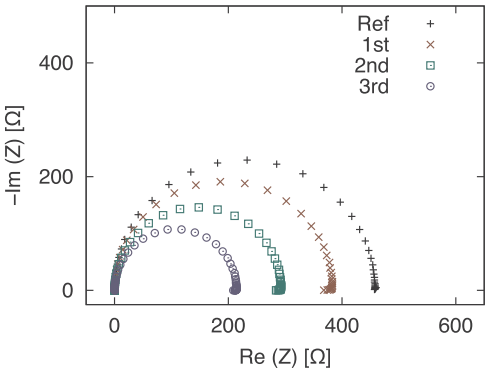

(b) Nyquist plots

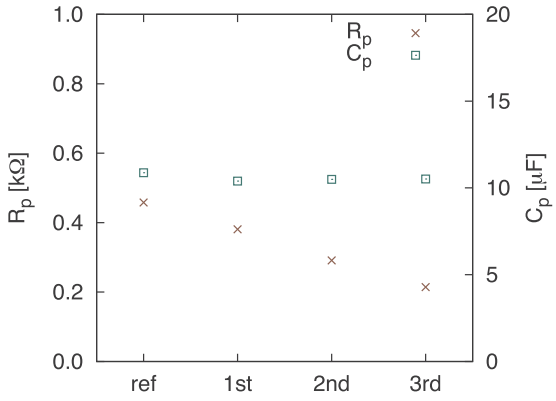

(c) Equivalent circuit parameters

Fig. 7. Nyquist plots, I-V curves, and equivalent circuit parameters for the polycrystalline silicon photovoltaic cell as a function of the number of times mechanical stress was applied.

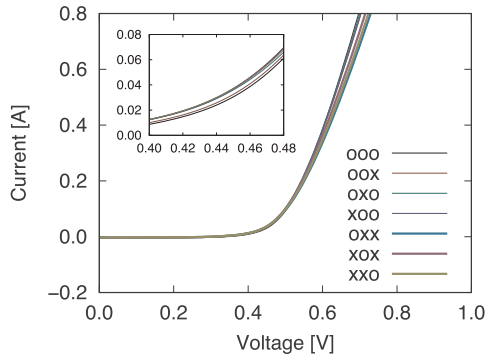

(a) I-V characteristics

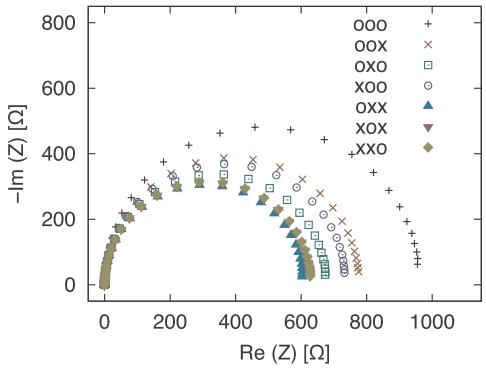

(b) Nyquist plots

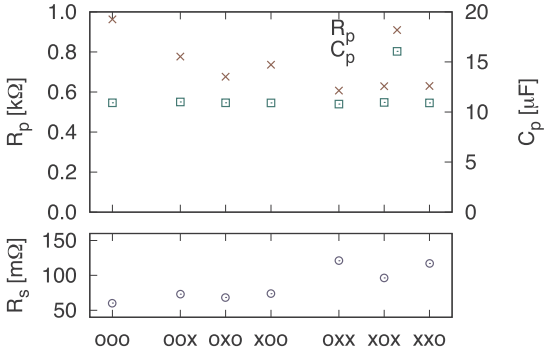

(c) Equivalent circuit parameters

Fig. 8. I-V curves, Nyquist plots and equivalent circuit parameters for the polycrystalline silicon photovoltaic cell when the interconnection ribbon connections are changed. “ooo” in the legends indicates all the wires are connected, while “oox” indicates the right wire of the three is disconnected.

[30], and explained to be the result of a negative constant phase element due to defects in the pn junctions of a Cu(In,Ga)Se_2 (CIGS) photovoltaic cell that they produced. A negative constant phase element is peculiar to defects in pn junctions; therefore, impedance spectroscopy can be used in practical application to differentiate such defects from other failures in a photovoltaic module.

4.2. Interconnect ribbon disconnection test

Fig. 8 shows the characteristics obtained when the number of connected wires were changed. Small voltage drops are observed in the larger current range due to concentration of the electric current path. The Nyquist plots appear to show larger differences than the I-V curves. Shrinkage of the semicircle in the Nyquist plot indicates a decrease in the parallel resistance, R_p. No negative constant phase element appears, unlike the Nyquist plots after the mechanical stress test. The decrease of R_p is attributed to current concentrated at a specific area. If interconnection ribbons are disconnected, then the current flow in the ribbons is stopped and the current starts to flow to other connected ribbons. The increased current in a specific area increases the voltage in that area, and R_p is decreased, as shown in Fig. 5 or Eq. (1). For the same reason, C_p is considered to be changed but is not actually changed. This is because, as shown in Fig. 5, the slope of C_p at a DC bias voltage of 0.1 V is small, which has only a small effect on C_p.

The series resistance R_s, indicates the bulk and wiring resistances, which includes the interconnection ribbons. Fig. 8 shows that an increase in the number of disconnected wires causes a higher R_s. As a matter of course, R_s is not changed in the case of semiconductor failure;

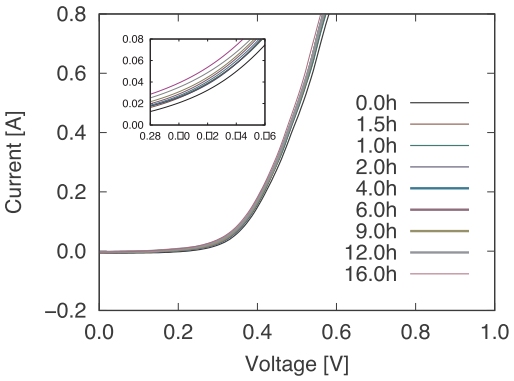

(a) I-V characteristics

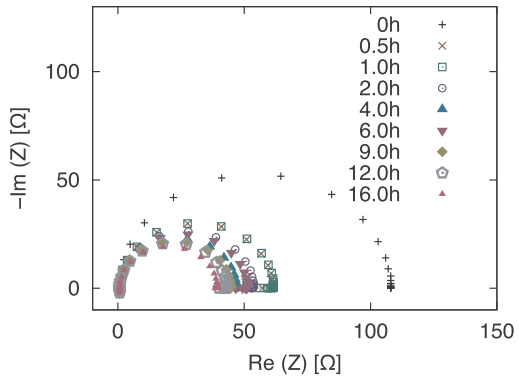

(b) Nyquist plots

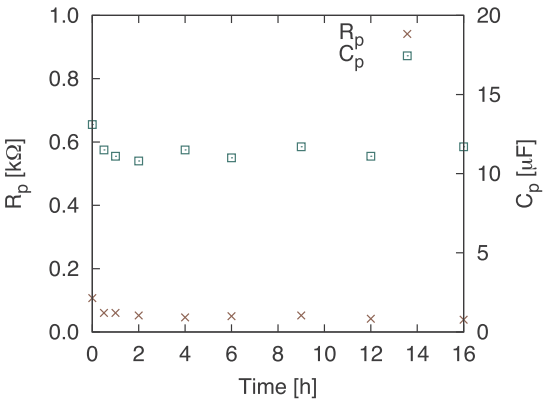

(c) Equivalent circuit parameters

Fig. 9. I-V curves, Nyquist plots and equivalent circuit parameters for the polycrystalline silicon photovoltaic cell during PID tests using white glass.

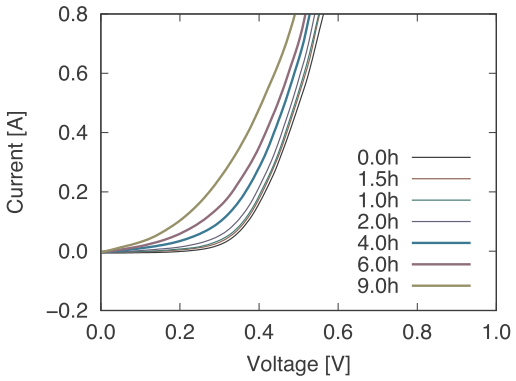

(a) I-V characteristics

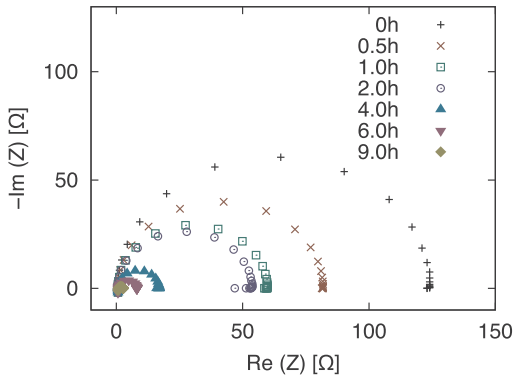

(b) Nyquist plots

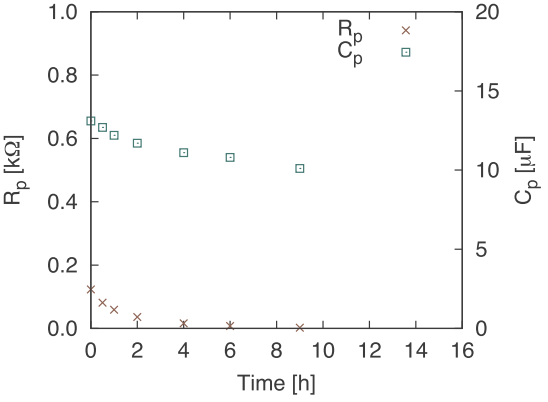

(c) Equivalent circuit parameters

Fig. 10. I-V curves, Nyquist plots and equivalent circuit parameters for the polycrystalline silicon photovoltaic cell during PID tests using soda-lime glass.

therefore, monitoring of R_s provides a means to detect interconnection ribbon failures and other wiring failures.

4.3. Potential-induced degradation test

Figs. 9 and 10 show time variations of the characteristics during the PID test using white glass and soda-lime glass, respectively. Both the I-V characteristics and the Nyquist plots obtained from the test with soda-lime glass were changed more significantly than those with the white glass. This is because soda-lime glass contains a larger amount of sodium ions, which diffuse into the pn junction and cause a leakage current. This is evidence that the experiment successfully reproduced PID in the cells. In particular, as shown in the I-V curves for soda-lime glass, the I-V characteristics gradually approach those of a pure resistance due to the leakage current. The leakage current is reflected in the decrease of R_p. Although a decrease in R_p is also observed in the mechanical stress test, the diffusion of sodium ions into the pn junction is the main factor that causes the decrease of R_p in this case. In the Nyquist plots, deformation derived from a negative constant phase element is also observed, similar to that in the mechanical stress test. This is because sodium ions diffuse in the photovoltaic cell and reach the pn junction.

It should be noted that, unlike the mechanical stress test, the parallel capacitance C_p is decreased with the PID intensity. C_p represents the capacitance that is formed in the depletion layer, and is influenced by the carrier density and other factors. We consider that the cause of the C_p decrease is that the diffusion of sodium ions changes the doping

condition in the pn junction, whereby the carrier density is decreased over the cell. Thus, the monitoring of C_p can help differentiate cell microcracks from PID if R_p is also decreased, which assists in identifying those cells in a photovoltaic module that are damaged.

5. Conclusion

Several types of failure and degradation in photovoltaic cells, such as mechanical stress, interconnect ribbon disconnection, and PID, were applied to photovoltaic modules. Nyquist plots of the photovoltaic cells were measured using impedance spectroscopy and compared with the IV characteristics of the modules. From the results of these analyses, the following conclusions were made: Mechanical stress decreases the parallel resistance and moves the low frequency range end of the Nyquist plot further inside the exact semicircle; the disconnection of interconnection ribbons decreases the parallel resistance and increases the series resistance; PID decreases both the parallel resistance and the capacitance. Based on these results, it has been demonstrated that these fault modes can be differentiated with Nyquist plots and the changes in the equivalent circuit parameters. Thus, the failures themselves and their fault modes are detectable using impedance spectroscopy.

In addition, the influence of the DC bias voltage and temperature on the impedance characteristics was investigated. The DC bias and the temperature affect both the parallel resistance and capacitance. Therefore, the DC bias voltage should be fixed carefully, and the equivalent circuit parameters obtained must be compensated according to the temperature for practical applications.

Acknowledgment

This work was supported by a Grant-in-Aid for Young Scientists (B) (No. 15K18027) from the Japan Society for the Promotion of Science (JSPS).

References

[1] P. Peng, A. Hu, W. Zheng, P. Su, D. He, K.D. Oakes, A. Fu, R. Han, S.L. Lee, J. Tang, Y.N. Zhou, Microscopy study of snail trail phenomenon on photovoltaic modules, RSC Adv. 2 (2012) 11357–11359, https://doi.org/10.1039/C2RA22280A.

[2] S. Meyer, S. Timmel, S. Richter, M. Werner, M. Glaser, S. Swatek, U. Braun, C. Hagendorf, Silver nanoparticles cause snail trails in photovoltaic modules, Sol. Energy Mater. Sol. Cells 121 (2014) 171–175, https://doi.org/10.1016/j.solmat.2013.11.013.

[3] A. Dolara, S. Leva, G. Manzolini, E. Ogliari, Investigation on performance decay on photovoltaic modules: snail trails and cell microcracks, IEEE J. Photovolt. 4 (2014) 1204–1211, https://doi.org/10.1109/JPHOTOV.2014.2330495.

[4] J. Chang, H. Yang, H. Wang, The investigation of snail trails in photovoltaic modules, in: Proceedings of the IEEE 42nd Photovoltaic Specialist Conference, 2015, 1–5. ⟨http://dx.doi.org/10.1109/PVSC.2015.7355713⟩.

[5] A. Meisel, Y. Xu, J. Fan, J. Wang, T. Dang, C. Alcantara, D. Inns, M. Terry, J. Kapur, B. Hamzavytehrany, W. Gambogi, H. Antoniadis, Holistic view of interactions in modules affecting durability-adhesion and snail trails, in: Proceedings of the 2015 IEEE 2nd Photovoltaic Specialist Conference, 2015, 1–4. ⟨http://dx.doi.org/10.1109/PVSC.2015.7355705⟩.

[6] G. Zhou, X. Xiong, W. Zhou, Y. Liu, Mechanism analysis of snail trails in photovoltaic modules, in: Proceedings of the IEEE 42nd Photovoltaic Specialist Conference, 2015, 1–4. ⟨http://dx.doi.org/10.1109/PVSC.2015.7355663⟩.

[7] A. Dolara, G.C. Lazaroiu, S. Leva, G. Manzolini, L. Votta, snail trails and cell microcrack impact on PV module maximum power and energy production, IEEE J. Photovolt. 4 (2016) 1–9, https://doi.org/10.1109/JPHOTOV.2014.2330495.

[8] T. Takashima, behavior of interconnect-failed pv modules under standard test conditions and actual operation conditions, IEEE J. Photovolt. 8 (2018) 1761–1766, https://doi.org/10.1109/JPHOTOV.2018.2868017.

[9] M.T. Zarmai, N.N. Ekere, C.F. Oduoza, E.H. Amalu, A review of interconnection technologies for improved crystalline silicon solar cell photovoltaic module assembly, Appl. Energy 154 (2015) 173–182, https://doi.org/10.1016/j.apenergy.2015.04.120.

[10] T.J. McMahon, Accelerated testing and failure of thin-film PV modules, Prog. Photovolt.: Res. Appl. 12 (2004) 235–248, https://doi.org/10.1002/pip.526.

[11] C. Brunetto, A. Moschetto, G. Tina, PEM fuel cell testing by electrochemical impedance spectroscopy, Electr. Power Syst. Res 79 (2009) 17–26, https://doi.org/10.1016/j.epsr.2008.05.012.

[12] P. Hacke, S. Spataru, K. Terwilliger, G. Perrin, S. Glick, S. Kurtz, J. Wohlgemuth, Accelerated testing and modeling of potential-induced degradation as a function of temperature and relative humidity, IEEE J. Photovolt. 5 (2015) 1549–1553, https://doi.org/10.1109/JPHOTOV.2015.2466463.

[13] P. Hacke, K. Terwilliger, R. Smith, S. Glick, J. Pankow, M. Kempe, S.K.I. Bennett, M. Kloos, System voltage potential-induced degradation mechanisms in PV modules and methods for test, in: Proceedings of the 37th IEEE Photovoltaic Specialists Conference, 2011, 000814–000820. ⟨http://dx.doi.org/10.1109/PVSC.2011.6186079⟩.

[14] N.C. Dong, M.A. Islam, Y. Ishikawa, Y. Uraoka, The influence of sodium ions decorated micro-cracks on the evolution of potential induced degradation in p-type crystalline silicon solar cells, Sol. Energy 174 (2018) 1–6, https://doi.org/10.1016/j.solener.2018.08.082.

[15] M. Schutze, M. Junghanel, M.B. Koentopp, S. Cwikla, S. Friedrich, J.W. Muller, P. Wawer, Laboratory study of potential induced degradation of silicon photovoltaic modules, in: Proceedings of the 2011 37th IEEE Photovoltaic Specialists Conference, 2011, 000821–000826. ⟨http://dx.doi.org/10.1109/PVSC.2011.6186080⟩.

[16] J. Bauer, V. Naumann, S. Grober, C. Hagendorf, M. Schutze, O. Breitenstein, On the mechanism of potential-induced degradation in crystalline silicon solar cells, Phys. Status Solidi Rapid Res. Lett. 6 (2012) 331–333, https://doi.org/10.1002/pssr.201206276.

[17] M. Schwark, K. Berger, R. Ebner, G. Ujvari, Investigation of potential induced degradation (PID) of solar modules from different manufacturers, in: Proceedings of the IECON 2013 – 39th Annual Conference of the IEEE, 2013, 8090–8097. ⟨http://dx.doi.org/10.1109/IECON.2013.6700486⟩.

[18] S. Hoffmann, M. Koehl, Effect of humidity and temperature on the potential-induced degradation, Prog. Photovolt.: Res. Appl. 22 (2014) 173–179, https://doi.org/10.1002/pip.2238.

[19] S. Pingel, O. Frank, M. Winkler, S. Daryan, Potential induced degradation of solar cells and panels, in: Proceedings of the 35th IEEE Photovoltaic Specialists Conference, 2010, 002817–002822. ⟨http://dx.doi.org/10.1109/PVSC.2010.5616823⟩.

[20] Y. Yang, D. Zhang, W. Guo, Virtual measurement of spacecraft solar array power loss in partially shaded condition, in: Proceedings of the 2015 IEEE International Conference on Computational Intelligence and Virtual Environments for Measurement Systems and Applications, 2015, 1–4. ⟨http://dx.doi.org/10.1109/CIVEMSA.2015.7158630⟩.

[21] A. Fezzani, I. Hadj Mahammed, S. Said, MATLAB-based modeling of shading effects in photovoltaic arrays, in: Proceedings of the 15th International Conference on Sciences and Techniques of Automatic Control and Computer Engineering, 2014, 781–787. ⟨http://dx.doi.org/10.1109/STA.2014.7086686⟩.

[22] D. Rossi, M. Omana, D. Giaffreda, C. Metra, modeling and detection of hotspot in shaded photovoltaic cells, IEEE Trans. VLSI Syst. 23 (2015) 1031–1039, https://doi.org/10.1109/TVLSI.2014.2333064.

[23] J. Hudson, L. Vasilyev, J. Schmidt, G. Horner, Economic impacts and approaches to address hot-spot defects in photovoltaic devices, in: Proceedings of the 35th IEEE Photovoltaic Specialists Conference, 2010, 001706–001709. ⟨http://dx.doi.org/10.1109/STA.2014.7086686⟩.

[24] T. Fuyuki, A. Kitiyanan, Photographic diagnosis of crystalline silicon solar cells utilizing electroluminescence, Appl. Phys. A 96 (2009) 189–196, https://doi.org/10.1007/s00339-008-4986-0.

[25] D. Hinken, K. Ramspeck, K. Bothe, B. Fischer, R. Brendel, Series resistance imaging of solar cells by voltage dependent electroluminescence, Appl. Phys. Lett. 91 (2007) 182104, https://doi.org/10.1063/1.2804562.

[26] M.K. Alam, F. Khan, J. Johnson, J. Flicker, PV ground-fault detection using spread spectrum time domain reflectometry (SSTDR), IEEE Energy Convers. Congr. Expo. (2013) 1015–1020, https://doi.org/10.1109/ECCE.2013.6646814.

[27] Review of Failures of Photovoltaic Modules, International Energy Agency Photovoltaic Power Systems Programme, 2014.

[28] M. Sugiyama, M. Hayashi, C. Yamazaki, N.B. Hamidon, Y. Hirose, M. Itagaki, Application of impedance spectroscopy to investigate the electrical properties around the pn interface of Cu(In,Ga)Se_2 solar cells, Thin Solid Films 535 (2013) 287–290, https://doi.org/10.1016/j.tsf.2012.11.070.

[29] M. Sugiyama, H. Sakakura, S.W. Chang, M. Itagaki, Investigation of sputtering damage around pn interfaces of Cu(In,Ga)Se_2 solar cells by impedance spectroscopy, Electrochim. Acta 131 (2014) 236–239, https://doi.org/10.1016/j.electacta.2014.04.058.

[30] H. Sakakura, M. Itagaki, M. Sugiyama, Estimation of defect activation energy around pn interfaces of Cu(In,Ga)Se_2 solar cells using impedance spectroscopy, Jpn. J. Appl. Phys. 55 (2015) 012301–012305, https://doi.org/10.7567/JJAP.55.012301.

[31] M.I. Oprea, S.V. Spataru, D.S. 2. I. 43rd, 2016, Detection of potential induced degradation in c-Si PV panels using electrical impedance spectroscopy, in: Proceedings of the IEEE 43rd Photovoltaic Specialists Conference, 2016, 5–10. ⟨http://dx.doi.org/10.1109/PVSC.2016.7749885⟩.

[32] T. Tanahashi, N. Sakamoto, H. Shibata, A. Masuda, Localization and characterization of a degraded site in crystalline silicon photovoltaic cells exposed to acetic acid vapor, IEEE J. Photovolt. 8 (2018) 997–1004, https://doi.org/10.1109/JPHOTOV.2018.2839259.